physica status solidi

pss

www.pss-journals.com

reprint

WILEY-VCH

Phys. Status Solidi C **12**, No. 4–5, 345–348 (2015) / **DOI** 10.1002/pssc.201400189

physica status solidi c
www.pss-c.com
current topics in solid state physics

Modeling micromechanical response to thermal history in bulk grown aluminum nitride

Payman Karvani and Antoinette M. Maniatty*

Department of Mechanical, Aerospace, and Nuclear Engineering, Rensselaer Polytechnic Institute, Troy, NY 12180, USA

Received 15 July 2014, revised 1 December 2014, accepted 1 March 2015
Published online 20 March 2015

Keywords AlN, constitutive model, crystal plasticity, wurtzite

* Corresponding author: e-mail maniaa@rpi.edu, Phone: +001-518-276-6984, Fax: +001-518-276-6025

A thermal-elastic-viscoplastic model suitable for modeling aluminum nitride (AlN) during crystal growth is presented. A crystal plasticity model that considers slip along crystallographic slip systems and the evolution of mobile and immobile dislocations on the prismatic and basal slip systems is developed. The model has been implemented into a finite element framework, and a sublimation growth process is modeled to demonstrate the model capability. The dislocation density, which characterizes the crystal quality, and the maximum tensile stress on the cleavage planes (m-planes), which leads to cracking, are computed.

1 Introduction Because of the great potential for new devices to be created based on high quality, single crystal, AlN substrates, tremendous research effort has been devoted to developing fabrication processes for its production [1,2]. However, the economical production of AlN substrates has been stymied by the challenges associated with the high temperature processes used to create them. Process modeling may be used to accelerate the advancement of these processes by allowing for new process designs and parameters to be tried out in simulation. Furthermore, while the opto-electronic properties of AlN are well-known, less is known about the thermal-mechanical behavior, particularly at high temperatures.

In this paper, an elastic-viscoplastic constitutive model for predicting the thermal-mechanical behavior of single crystal AlN at growth temperatures is presented. The model explicitly considers the wurtzite crystal structure of AlN and the processes of dislocation multiplication, motion, and interaction on the basal and prismatic slip systems. The model has been implemented into a finite element framework, and preliminary results demonstrating the ability of the model to predict key parameters associated with defects, specifically dislocation density and the tensile stress on the cleavage planes that leads to cracking.

2 Thermal-mechanical governing equations The thermal-mechanical behavior is governed by the equilibrium equation combined with a kinematic equation relating displacement and strain, and constitutive equations relating the temperature and stress to the strain. Assuming small strains, quasi-static conditions, and neglecting body forces, the governing equations are

$$\nabla \cdot \boldsymbol{\sigma} = 0\,, \tag{1}$$

$$\boldsymbol{\varepsilon} = \frac{1}{2}\left(\nabla \boldsymbol{u} + \nabla \boldsymbol{u}^T\right) = \boldsymbol{\varepsilon}^\theta + \boldsymbol{\varepsilon}^e + \boldsymbol{\varepsilon}^p\,, \tag{2}$$

$$\boldsymbol{\varepsilon}^\theta = \int_{\theta_0}^{\theta_f} \boldsymbol{\alpha}(\theta)\, d\theta\,, \tag{3}$$

$$\boldsymbol{\sigma} = \boldsymbol{\mathcal{C}}(\theta) : \boldsymbol{\varepsilon}^e\,, \tag{4}$$

where $\boldsymbol{\sigma}$ is the stress tensor, which must satisfy equilibrium (Eq. (1)); $\boldsymbol{\varepsilon}$ is the strain tensor, which is assumed to follow an additive decomposition into thermal $\boldsymbol{\varepsilon}^\theta$, elastic $\boldsymbol{\varepsilon}^e$, and plastic $\boldsymbol{\varepsilon}^p$ parts (Eq. (2)); $\boldsymbol{u}$ is the displacement vector field; $\boldsymbol{\alpha}$ is the thermal expansion tensor which depends

on the temperature θ; θ_0 and θ_f are the initial and final temperatures; and $\boldsymbol{\mathcal{C}}$ is the temperature dependent fourth order elasticity tensor. The constitutive behavior relating the plastic strain $\boldsymbol{\varepsilon}^p$ and the stress $\boldsymbol{\sigma}$ remains to be defined, and is described in Section 3. In addition to the governing equations, boundary conditions are required, which are described in Section 4.

The thermal and elastic strain behavior has been measured experimentally. The thermal expansion tensor $\boldsymbol{\alpha}$ for hexagonal materials has only two independent components, along the lattice a directions, α_a, and the lattice c direction, α_c. The components of the tensor also depend on the orientation of the lattice relative to the global reference frame, which is assumed known. The linear thermal expansion of AlN in both directions has been estimated by Reeber and Wang [3] using available experimental data [4, 5] and a semi-empirical method up to 2000 K. That data is used in this work for modeling thermal expansion in the AlN.

For hexagonal symmetry, there are only five independent components of the fourth order elasticity tensor $\boldsymbol{\mathcal{C}}$. Pandey and Yadav [6] measured the AlN elastic moduli over a temperature range of 200–800 K. Those data are fit to quadratic curves and extrapolated to growth temperatures in this work.

In addition to the AlN, it is important to model the material that supports the AlN during the growth process. Polycrystalline tungsten (W) is assumed to be the crystal-holder material in sublimation growth here. The polycrystalline W crystal-holder is treated as as isotropic, thermal-elastic. The temperature dependent thermal expansion coefficient was measured by Dubrovinsky and Saxena [7], and the temperature dependent elastic properties can be found in Lassner and Schubert [8].

3 Crystal viscoplastic model While the thermal and elastic parts of the strain in Eq. (2) are fairly well-defined for AlN, no experimental stress-strain data is available to fit a viscoplastic material model. Furthermore, the plastic strain $\boldsymbol{\varepsilon}^p$ depends on the history of the stress and temperature, and is associated with the micromechanical mechanism of dislocation motion on crystallographic slip systems and the evolution of dislocation density. In this work, we expand and modify the model originally developed by Alexander and Haasen [9] The three prismatic $<11\bar{2}0>\{1\bar{1}00\}$ and three basal $<11\bar{2}0>(0001)$ slip systems, which are the primary slip systems for AlN, are considered.

The equations relating the plastic strain to the stress for multi-slip crystal plasticity used here are

$$\dot{\boldsymbol{\varepsilon}}^p = \sum_{\beta=1}^{n_s} \frac{1}{2}\dot{\gamma}^\beta \left(\boldsymbol{s}^\beta \otimes \boldsymbol{m}^\beta + \boldsymbol{m}^\beta \otimes \boldsymbol{s}^\beta\right) , \tag{5}$$

$$\dot{\gamma}^\beta = \rho_m^\eta \, b v_o \exp\left(\frac{-Q^\eta}{k\theta}\right)\left(\frac{|\tau^\beta|}{\hat{\tau}^\eta}\right)^{\frac{1}{m}} sgn\left(\tau^\beta\right) , \tag{6}$$

$$\tau^\beta = \boldsymbol{s}^\beta \cdot (\boldsymbol{\sigma} \cdot \boldsymbol{m}^\beta) , \tag{7}$$

$$\hat{\tau}^\eta = \hat{\tau}_f^\eta + f\, G^\eta\, b\sqrt{\rho_f^\eta} . \tag{8}$$

Equation (5) is a kinematic equation relating the rate of shearing $\dot{\gamma}^\beta$ on each slip system β to the plastic strain rate, where $n_s = 6$ is the total number of slip systems considered and $\boldsymbol{m}^\beta$ and $\boldsymbol{s}^\beta$ are the slip plane normal and slip direction, respectively. Equation (6) is based on Orowan's equation [10] and assumes a power law relationship between the resolved shear stress τ^β and the rate of shearing, where superscript η indicates slip system type ($\eta = p$ for prismatic and $\eta = b$ for basal), ρ_m^η is the mobile dislocation density, b is the Burgers vector length, v_o is a reference dislocation velocity, Q^η is the activation energy for dislocation glide, k is Boltzmann's constant, $\hat{\tau}^\eta$ is the resistance to slip, and m is the empirical strain rate sensitivity. The function sgn returns the sign of its argument ensuring the direction of slip is in the direction of the resolved shear stress. In Eq. (6), an average, effective dislocation velocity is assumed, combining the different parts of a dislocation loop, with different line directions, into a single term. This assumes that the activation energy for dislocation segments of different character is the same, and thus, a constant relative mobility of the different segments. This is consistent with the observation of predominantly long screw segments from room temperature to 800 °C by Audurier et al. [11], although they also observed an apparent change in the relative mobility of edge dislocations on the prismatic planes, which is not captured in this model. Eq. (8) defines the resistance to slip in terms of a constant lattice friction stress $\hat{\tau}_f^\eta$ and a hardening term associated with the immobile dislocation density ρ_f^η, where f is a coefficient typically taken to be 1/3, and G^η is the elastic shear modulus, $G^b = C_{44}$ for basal slip and $G^p = \frac{1}{2}(C_{11} - C_{12})$ for prismatic slip.

In addition to modeling slip on multiple slip systems, this model is different from the classic model proposed by Alexander and Haasen [9] in three other key respects: (1) the immobile and mobile dislocation density are considered separately, (2) a friction stress is included in Eq. (8), and (3) the hardening is incorporated in the denominator of Eq. (6) rather than as a back stress. The mobile and immobile dislocations are considered separately here because the mobile dislocations act to enable slip, while the immobile dislocations act to hinder slip, effectively strengthening the material, and while they are related, they evolve differently [12]. The friction stress is added to consider the resistance of the crystal lattice to dislocation motion in addition to the immobile dislocation obstacle term. Frost and Ashby [13] suggest at temperatures above 40% of the melt temperature, dislocation glide by power law creep, of the form

in Eq. (6), is the dominant mechanism in ceramics. In Maniatty and Karvani [15], the power law relationship given in Eq. (6), is compared to that using a back stress, and the results are found to be nearly identical.

In addition to Eqs. (5)–(8), evolution equations for the mobile and immobile dislocations densities are required. In this work, we use dislocation density evolution equations similar to those proposed by Kubin and Estrin [12] of the form

$$\dot{\rho}_m = \left[\frac{g_1}{b^2} - g_2\,\rho_m - \frac{g_3}{b}\sqrt{\rho_f}\right]\dot{\gamma}\,, \tag{9}$$

$$\dot{\rho}_f = \left[g_2\,\rho_m + \frac{g_3}{b}\sqrt{\rho_f}\right]\dot{\gamma}\,, \tag{10}$$

where $g_1 - g_3$ are dimensionless constants. The first term in Eq. (9) is the dislocation multiplication term, and the last two terms are associated with the trapping of mobile dislocations by other mobile and immobile dislocations. Those immobilized dislocations then appear as the terms in Eq. (10).

Lastly, it remains to determine the model parameters. Currently, there is no stress-strain data for AlN at elevated temperatures with which to fit the model parameters. Yonenaga and Motoki [14] performed compression tests on single crystal GaN samples oriented for prismatic slip at three different temperatures. From that data, it was possible to determine the model parameters for prismatic slip in GaN [15]. GaN and AlN both have a wurtzite crystal structure and similar lattice parameters. It is expected, their viscoplastic properties would be similar, and thus, most of the model parameters are assumed to be the same. Specifically, the model is relatively insensitive to the reference dislocation velocity, v_o, and this is set to $v_o = 10^3$m/s, which is on the order of the elastic wave speeds. The activation energy for dislocation glide, Q^p, is typically proportional to $G_0 b^3$, where G_0 is the shear modulus at 300K [13], and $G_0 b^3$ is nearly equivalent in AlN and GaN, thus, the same activation energy is assumed. However, the AlN is observed to be roughly 50% stronger than GaN in Yonenaga *et al.* [16], who present comparative hardness test data over a wide temperature range. The friction stress, $\hat{\tau}_f^p$ which governs initial yield, is set 50% higher in AlN than in GaN. No information is available regarding the rate sensitivity or hardening behavior, and thus, those parameters are set equal in AlN to those found for GaN. Lastly, the parameters must also be specified for basal slip. Audurier *et al.* [11] observed dislocations in about equal proportion on basal and prismatic slip systems in polycrystalline AlN, and thus, equal parameters are assumed for basal and prismatic slip. The parameters are summarized in Table 1.

Table 1 Model parameters for AlN.

Q (eV)	m	$\hat{\tau}_f$	g_1 ($\times 10^{-6}$)	g_2 ($\times 10^{3}$)	g_3 ($\times 10^{-5}$)
2.02	0.265	78.3	0.5	0.7	3.2

4 Finite element model of sublimation growth

The governing equations and constitutive model described in the preceding sections has been implementing into a three-dimensional finite element framework. Quadratic tetrahedral elements with ten nodes are used.

To model sublimation growth, the W crystal-holder together with the AlN crystal are modeled as solid cylindrical disks. The crystal-holder is 1 mm thick and 60 mm in diameter, and the AlN crystal is 10 mm thick and 50 mm in diameter. The AlN crystal is grown along the c-direction, aligned with the z-axis. The bottom and cylindrical surfaces of the AlN crystal are traction-free and the top is perfectly bonded to the W crystal-holder. The top of the crystal holder is fixed in the vertical direction at the center and at one point on the outer radius to prevent rigid body motion but allow bending of the crystal-holder. Because of symmetry, only one fourth of the model needs to be considered consisting of about 37000 elements, and with symmetric boundary conditions. The model is subjected to a temperature field history that approximately models the crystal cool-down process from growth temperature of 2500 K. The temperature field history is stated as a function of r and z: radial distance from the axis of symmetry and distance from the interface of crystal with the crystal-holder.

$$\theta(r,z,t) = (a_0 + a_1 r + a_2 z + a_3 r z)\,(1 - \frac{t}{t_f}) + \frac{t}{t_f}\theta_o\,, \tag{11}$$

where θ_o is room temperature, t_f is the cool-down time, a_0 is the temperature in the middle of the crystal at the interface with the crystal-holder, a_1 is the radial temperature gradient in the crystal at the interface with the crystal-holder, and a_2 is the axial temperature gradient along the axis of symmetry. a_3 determines how radial and axial temperature gradients vary within the crystal. The values of these parameters are based on the upper limit of temperature gradients within the growth cell, reported in a recent patent [17].

5 Results Of primary interest is to predict the likelihood of cracking and dislocation density due to the thermal stresses arising as the crystal is cooled from the growth temperature. The maximum tensile stress on the cleavage planes, which has a strong correlation with cracking, is illustrated in Fig. 1. The stress concentration near top of the crystal at the interface with crystal-holder is due to mismatch in the thermal expansion coefficients of AlN and W, which is about 2×10^{-6} K^{-1} at its peak. The stress near the bottom of the crystal is due to high temperature gradients, in this case 40 °C/cm and 10 °C/cm in the radial and axial directions, respectively.

The dislocation density in the AlN crystal, which is initially set to 10^3 cm^{-2}, does not evolve significantly, less than one order of magnitude, as shown in Fig. 2. The maximum mobile dislocation density is predicted to be 10^4

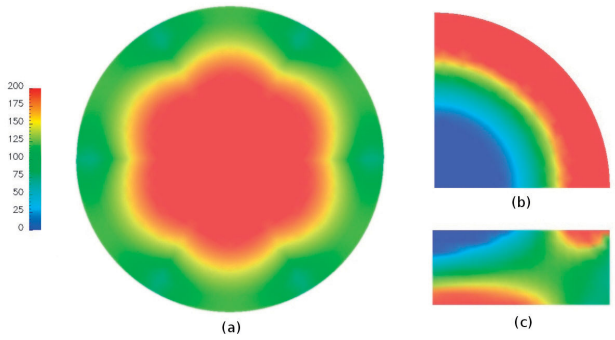

Figure 1 Estimated maximum tensile stress (MPa) on the cleavage planes in the AlN crystal: (a) bottom view indicating hexagonal symmetry, (b) top view, and (c) side view. Maximum stress is 450 MPa and appears at a tiny region on the top edge of crystal. The W crystal-holder is not shown.

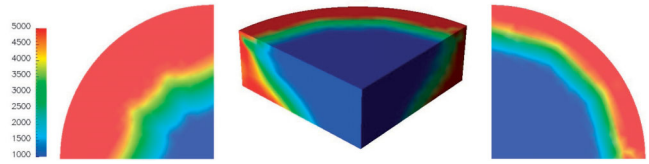

Figure 2 Estimated dislocation density (cm^{-2}) in AlN crystal grown with sublimation method. From left to right: bottom view, 3D view of $\frac{1}{4}$ sample, and top view. Dislocation density at bottom edge is highly localized with maximum value of 10^4 cm^{-2}. The W crystal-holder is not shown.

cm^{-2}, while the maximum immobile dislocation density is 5×10^3 cm^{-2}. Basal dislocations evolve more quickly near the top edge of crystal at the interface with the crystal-holder, while dislocation density on prismatic slip systems tends to occur near the bottom edge of the crystal. The plastic slip on prismatic slip system is more sensitive to temperature gradients, while the plastic slip on the basal slip systems is mainly due to the mismatch in the thermal expansion coefficients of AlN and W.

6 Conclusions The developed thermal-mechanical model for AlN crystals at growth temperatures provides insight into the sources of thermal stress that lead to cracking and dislocations in AlN crystals grown by sublimation. This work shows that the mismatch in the thermal expansion coefficient between the AlN crystal and the W crystal-holder is the primary source of stress, with temperature gradients having a smaller contribution. As a result, the maximum tensile stress on the cleavage planes, which leads to cracking, occurs at the interface between the AlN crystal and the W crystal-holder. Furthermore, the model predicts relatively little growth in the dislocation density, which is consistent with the small dislocation densities observed in AlN crystals grown by sublimation. Dislocations are predicted to be primarily on the basal slip systems near the interface between the AlN crystal and crystal-holder. The presented model parameters and simulations based on these model parameters have significant uncertainty because of the lack of experimental data to characterize the thermal-mechanical behavior of AlN, necessary for model calibration. However, the model is expected to predict the correct trends, and results are consistent with experimental observations. Thus, the model can be used for AlN semiconductor process design.

Acknowledgements This work was supported by the National Science Foundation under Grant No. CMMI-0928556. The authors acknowledge many helpful discussions with Dr. R. Bondokov and Dr. L. Schowalter of Crystal IS, Inc. The simulations presented were carried out on the Blue Gene/Q at the Center for Computational Innovations at Rensselaer.

References

[1] R. T. Bondokov, S. G. Mueller, K. E. Morgan, G. A. Slack, S. B. Schujman, M. C. Wood, J. A. Smart, and L. J. Schowalter, J. Cryst. Growth **310**, 4020 (2008).
[2] T. Morishita, M. Iwaya, T. Takeuchi, S. Kamiyama, and I. Akasaki, J. Cryst. Growth **390**, 45 (2014).
[3] R. R. Reeber and K. Wang, Mater. Res. Soc. Symp. **622**, T6.35.1 (2000).
[4] W. M. Yim and R. J. Paff, J. Appl. Phys. **45**, 1457 (1974).
[5] G. A. Slack and S. F. Bartram, J. Appl. Phys. **46**, 89 (1975).
[6] D. Pandey and R. Yadav, Appl. Acoustics **70**, 412 (2009).
[7] L. S. Dubrovinsky and S. K. Saxena, Phys. Chem. Minerals **24**, 547 (1997).
[8] E. Lassner and W. Schubert, Tungsten: Properties, Chemistry, Technology of the Elements, Alloys, and Chemical Compounds (Plenum Press, New York, 1999).
[9] H. Alexander and P. Haasen, in: Adv. Solid State Phys., Vol. 22, edited by F. Sietz, D. Turnbull, and H. Ehrenreich (Academic Press, London, 1968), p. 27.
[10] E. Orowan, Phys. Soc. Proc. **52**, 8 (1940).
[11] V. Audurier, J. L. Demenet, and J. Rabier, Philos. Mag. A **77**, 825 (1998).
[12] L. P. Kubin and Y. Estrin, Acta Metall. Mater. **38**, 697 (1990).
[13] H. J. Frost and M. F. Ashby, Deformation Mechanism Maps (Pergamon Press, New York, 1982).
[14] I. Yonenaga and K. Motoki, J. Appl. Phys. **90**, 6539 (2001).
[15] A. Maniatty and P. Karvani, J. Eng. Mater. Technol. **137**, 1 (2015).
[16] I. Yonenaga, A. Nikolaev, Y. Melnik, and V. Dmitriev, J. Appl. Phys. **40**, L426 (2001).
[17] R. T. Bondokov, S. P. Rao, S. R. Gibb, and L. J. Schowalter, U.S. Patent No. 20,120,000,414 (2012).

